Excitation cross sections for krypton by electrons in the 15–100-eV impact-energy range

S. Trajmar, S. K. Srivastava, H. Tanaka,* and H. Nishimura†
California Institute of Technology, Jet Propulsion Laboratory, Pasadena, California 91103

D. C. Cartwright
Theoretical Division, Los Alamos Scientific Laboratory, University of California, Los Alamos, New Mexico 87645
(Received 13 May 1980)

Differential, integral, and momentum-transfer cross sections have been determined for the excitation of the 24 lowest electronic states of Kr (some of the transitions are unresolved). The inelastic-scattering cross sections were normalized to the absolute scale with the help of the elastic-scattering differential cross sections (DCS's) which in turn were normalized with respect to absolute He DCS's. The impact energies were 15, 20, 30, 50, and 100 eV and the DCS's were obtained over the range of 5°–135° scattering angles. The error limits associated with the differential, integral, and momentum-transfer cross sections have been estimated at 25%, 38%, and 46%, respectively.

I. INTRODUCTION

High-efficiency lasing in KrF has been demonstrated by utilizing both direct electron beam pumping[1] and electron beam stabilized discharge pumping[2] of argon-krypton-fluorine mixtures but the role of the excited states of the inert gas atom in these lasers is still not understood. An extensive study of Ar and Kr was, therefore, undertaken to obtain the electron-impact excitation cross sections which are necessary to construct a better model of the laser systems involving these atoms. The elastic-scattering measurements have been summarized by Srivastava *et al.*,[3] and the Ar inelastic cross sections by Chutjian and Cartwright.[4] The present paper reports Kr inelastic cross sections. This is the least studied atom among the rare gases (except Rn) and is, therefore, also of interest for completing a systematic survey of the electron rare-gas electron scattering processes.

Earlier measurements on total scattering cross sections were done by Ramsauer[5] and Ramsauer and Kollath[6] and the results have been summarized by Massey *et al.*[7] More recently, Schaper and Scheibner[8] utilized an improved Maier-Leibnitz collision chamber to obtain total excitation cross sections from threshold to 14-eV impact energies. Wagenaar[9] remeasured the total cross sections from 22.5- to 750-eV impact energies. A summary of total scattering, excitation, ionization, and elastic cross sections based on a semiempirical method and all available data from 20- to 3000-eV impact energies was given by de Heer *et al.*[10] Only a very limited amount of work has been done with the aim of obtaining differential cross sections (DCS) for individual excitation processes and for optical f values of Kr. Lewis *et al.*[11] measured the angular distributions for the $4p$-$5s$ (unresolved) excitation at 50 and 60 eV and normalized their relative cross sections to results obtained from an optical-model theory.[12] Delage and Carette[13] measured the 0° and 30° inelastic-scattering intensity ratios (with respect to the $5s[1\frac{1}{2}]_1$ excitation) for a number of states as a function of impact energy in the 15 to 400 and 15 to 80-eV energy ranges, respectively. They also determined the angular dependence of these same ratios at 15 and 60 eV impact energies in the 0° to 90° and 0° to 60° angular ranges, respectively. The same authors[14] have derived relative effective oscillator strengths for 9 excitations from their energy-loss spectra obtained in the 15 to 400-eV energy range and 0° to 90° angular regions. The effective generalized oscillator strengths were extrapolated to zero momentum transfer and the limit values were normalized to the optical f values of Ganas and Green.[15] More recently Delage and Carette[16] determined relative differential cross sections for a number of excitation processes in the 15-to 100 eV impact energy and 2° to 90° angular ranges. The optical f values for the $5s[1\frac{1}{2}]_1$ and $5s'[0\frac{1}{2}]_1$ excitations have been measured by Geiger[17] utilizing high energy (36 KeV), high-resolution electron spectroscopy. De Jongh and Van Eck[18] determined the optical oscillator strengths for the $5s'[0\frac{1}{2}]_1$ excitation by measureing the self-absorption of radiation as a function of gas pressure.

Theoretical calculations have been limited to those of Ganas and Green[15] who calculated integral cross sections for the $4p \rightarrow 5s$ optically allowed transitions with a Born-type approximation and with semiempirical distortion corrections. In this paper we report differential, integral, and momentum-transfer cross sections for the excitation of 19 individual or composite electronic states lying below 12.40 eV and compare them with available earlier results.

II. EXPERIMENTAL APPARATUS AND PROCEDURES

The electron-impact spectrometer and the experimental procedures utilized in obtaining the

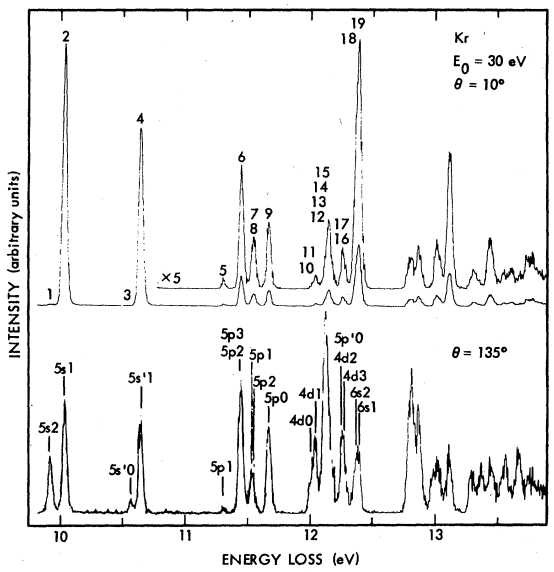

FIG. 1. Energy-loss spectra of Kr at 30-eV impact energy and 10° and 135° scattering angles. The feature numbers are indicated in the upper spectrum and the designation with J values in the lower spectrum. (See Table I for the explanation of the designations.)

present results have been described previously.[19,20] The target Kr beam was generated by a capillary array and crossed with an electron beam of about 40-meV full width at half maximum (FWHM). The inelastically scattered signal intensity as a function of energy loss (ΔE) was recorded at fixed impact energies (E_0) and scattering angles (θ) utilizing pulse counting and multichannel scaling techniques. Typical energy-loss spectra are shown in Fig. 1, an energy level diagram is given in Fig. 2, and the notations are summarized in Table I.

From the energy-loss spectra, the relative intensities of the individual features with respect to the $5s[1\frac{1}{2}]_1$ excitation feature were determined by utilizing a computer unfolding procedure.[21] The relative intensities are equal, to a very good approximation, to the relative differential cross sections.

In a separate series of experiments the intensity of the $5s[1\frac{1}{2}]_1$ excitation with respect to elastic-scattering intensity was measured. This ratio again is equal (to a good approximation) to the ratio of the respective DCS's. The elastic DCS measured recently by Srivastava *et al.*[3] were

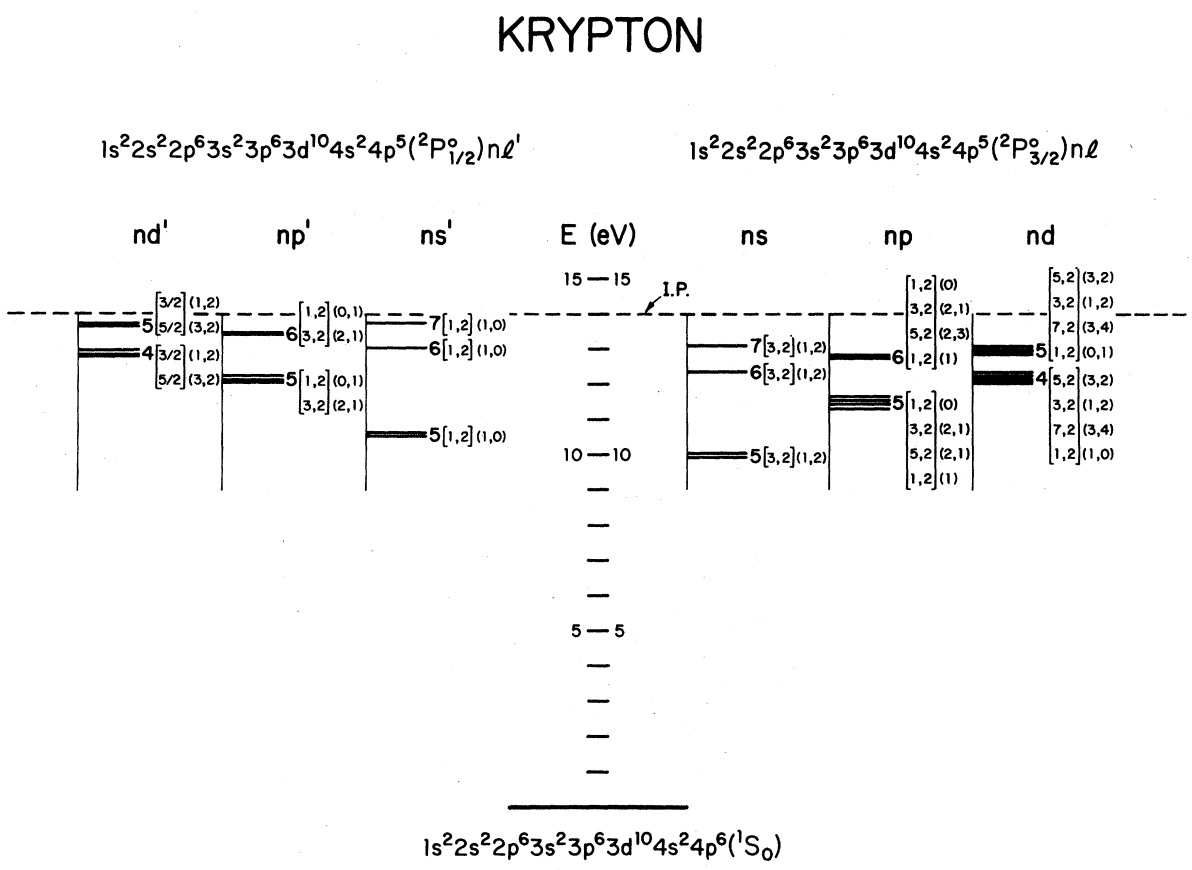

FIG. 2. Energy level diagram for Kr.

TABLE I. List of energy levels of Kr and their designations. (Energy levels joined by square brackets were treated as one level in the computer unfolding procedure. The intensities associated with energy levels joined by curly brackets were added together in the final summary of differential cross sections.)

Feature No.[a]	Designation[b]	J	Energy (eV)	Designation[c]
Ground state	$4p^6\,{}^1S$	0	0.0	
1	$5s[1\frac{1}{2}]$	2	9.915	A
2	$5s[1\frac{1}{2}]$	1	10.033	B
3	$5s'[0\frac{1}{2}]$	0	10.563	C
4	$5s'[0\frac{1}{2}]$	1	10.644	D
5	$5p[0\frac{1}{2}]$	1	11.304	E
6	$5p[2\frac{1}{2}]$	3	11.443	F
	$5p[2\frac{1}{2}]$	2	11.445	
7	$5p[1\frac{1}{2}]$	1	11.526	
8	$5p[1\frac{1}{2}]$	2	11.546	G
9	$5p[0\frac{1}{2}]$	0	11.666	H
10	$4d[0\frac{1}{2}]$	0	11.998	
11	$4d[0\frac{1}{2}]$	1	12.037	I
12	$5p'[1\frac{1}{2}]$	1	12.101	
13	$4d[1\frac{1}{2}]$	2	12.112	
	$4d[1\frac{1}{2}]$	4	12.126	
14	$5p'[0\frac{1}{2}]$	1	12.141	J
	$5p'[1\frac{1}{2}]$	2	12.144	
15	$4d[3\frac{1}{2}]$	3	12.179	
16	$5p'[0\frac{1}{2}]$	0	12.257	K
	$4d[2\frac{1}{2}]$	2	12.258	
17	$4d[2\frac{1}{2}]$	3	12.284	
18	$6s[1\frac{1}{2}]$	2	12.352	L
	$4d[1\frac{1}{2}]$	1	12.355	
19	$6s[1\frac{1}{2}]$	1	12.386	

[a] Number refers to our designation Fig. 1 and Tables I–V.

[b] j-l coupling notation used by C. E. Moore (Circular of the National Bureau of Standards 467, Aug. 15, 1952).

[c] Designation used by Delage and Carette (Refs. 13 and 14).

utilized together with the intensity ratios to obtain absolute DCS for the $5s[1\frac{1}{2}]_1$ excitation. A combination of this DCS with the relative inelastic intensities, obtained from the energy-loss spectra, then yielded all inelastic cross sections in absolute units.

The $5s[1\frac{1}{2}]_1$ excitation to elastic-scattering intensity ratios have been measured in the angular range of $10° < \theta < 135°$ at 15 and 20 eV impact energies and in the $5° < \theta < 135°$ range at 30, 50, and 100-eV impact energies. The upper limit in the angular range is set by the geometry of the apparatus and the lower limit by the interference of the direct beam with the elastic signal.

The impact-energy scale was calibrated against the 19.35-eV He resonance in the elastic channel at 90°. The true zero scattering angle was determined from the symmetry of elastic scattering around the nominal zero degree angle.

III. RESULTS AND DISCUSSION

A. Calibration of the $5s[1\frac{1}{2}]_1$ excitation cross section against elastic scattering

The relative scattering intensity of the $5s[1\frac{1}{2}]$ excitation (feature 2, see Table I) with respect to

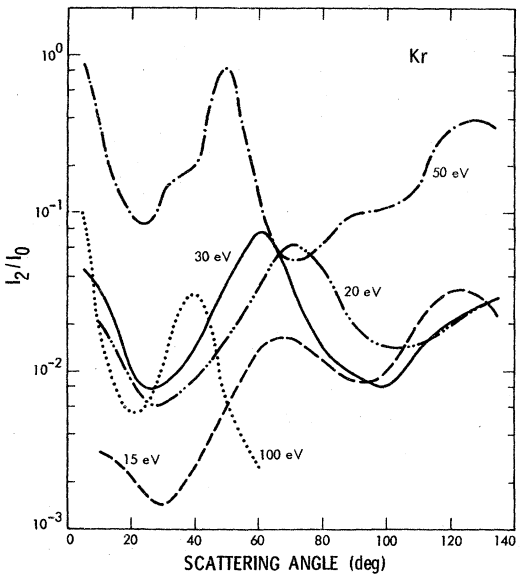

FIG. 3. Relative scattering intensities for the $5s[1\frac{1}{2}]_1$ excitation (feature 2) with respect to elastic scattering at 15-, 20-, 30-, 50-, and 100-eV impact energies.

elastic scattering was determined at each impact energy as a function of the scattering angle. The smooth curves drawn through the experimental points are shown in Fig. 3. In the 10° to 20° region for 15- and 20-eV impact energies and in the 5° to 10° region for the 30-, 50-, and 100-eV impact energies the elastic-scattering intensity and therefore the inelastic to elastic intensity ratios may have been influenced somewhat by direct beam contribution. Below 10° (or 5° for the higher energies) this contribution to the measured signal becomes substantial and therefore no elastic-scattering measurements were feasible with the apparatus at these angles.

Utilizing the intensity ratios represented by the smooth curves in Fig. 3 and the elastic DCS of Srivastava *et al.*,[3] the DCS for excitation of the $5s[1\frac{1}{2}]_1$ state was obtained at each impact energy. Srivastava *et al.* published elastic DCS's only at angles ranging from 20° to 135°. We obtained the 10° elastic DCS's by extrapolation from their data. The results are summarized in Tables II through VI and shown for 15 and 100 eV in Figs. 4 and 5. The relative DCS values of Delage and Carette[16] (15, 20, 30, 50, and 100 eV) have been normalized to the present data at one angle. In general, the shapes of the angular distributions are in good agreement except for the 90° values. At this angle, the results of Delage and Carette (15 and 20 eV) are considerably lower than the present values (see Fig. 4).

B. Relative inelastic-scattering intensities

Typical energy-loss spectra obtained at 30 eV impact energy and at 10° and 135° scattering angles are shown in Fig. 1. For the computer unfolding of the experimental spectra, 19 features were specified five of which represent experimentally unresolvable pairs (features 6, 13, 14, 16, and 18 in Table I). It was found, however, that some of the 19 features were significantly overlapped and the separation of them into individual intensities resulted in large uncertainties. To avoid this problem, the intensities of these overlapping features were combined into composite intensities as indicated in the first column of Table I. Twelve individual intensities were thus generated: six of them (features 1, 2, 3, 4, 5, and 9) represent individual transitions, two represent the overlap of two transitions (7, 8 and 10, 11), two represent the overlap of three transitions (16, 17 and 18, 19), and one represents the overlap of six transitions

TABLE II. Differential cross sections at 15-eV impact energy. See Table I for the designations.

θ (deg)	DCS (10^{-19} cm^2/sr)											
	1	2	3	4	5	6	7+8	9	10+11	12+13+14+15	16+17	18+19
10	1.9	48	1.34	24	5.8	5.3	1.9	1.4	0.5	5.8	0.96	1.4
20	3.1	28	0.56	15.1	3.9	6.2	3.1	1.1	0.7	5.0	2.0	1.7
30	3.6	15	0.35	8.0	1.50	5.7	2.7	0.9	0.7	4.1	1.4	1.4
40	4.0	11.5	0.47	6.6	0.69	5.3	1.6	1.0	0.8	4.4	1.0	1.6
50	4.4	10.2	0.73	6.2	0.82	5.3	1.1	1.2	1.1	5.3	0.9	2.0
60	4.7	9.4	0.99	6.3	1.03	5.6	1.1	1.7	1.3	6.4	1.5	2.5
70	4.9	7.0	0.88	4.8	0.77	3.8	1.0	1.7	1.2	5.3	1.6	2.4
80	3.5	4.5	0.59	3.2	0.34	2.2	0.8	1.6	0.9	4.5	1.4	1.8
90	2.7	3.8	0.48	2.9	0.23	1.4	1.0	1.5	0.8	4.4	1.6	1.5
100	2.3	4.4	0.46	3.4	0.42	1.1	1.1	0.7	0.8	4.8	1.9	1.3
110	2.7	5.3	0.51	4.1	1.11	1.3	1.2	0.16	0.8	5.0	1.2	1.3
120	3.9	7.0	0.70	5.5	1.96	2.0	1.6	0.28	1.2	5.9	1.05	1.8
130	5.0	9.0	0.90	7.0	2.1	3.2	2.4	1.26	2.6	7.2	1.4	2.8
135	5.5	10.0	1.00	7.9	1.80	4.2	2.9	2.4	3.4	8.0	2.0	3.5

TABLE III. Differential cross sections at 20-eV impact energy. See Table I for the designations.

θ (deg)	DCS (10^{-19} cm^2/sr)											
	1	2	3	4	5	6	7+8	9	10+11	12+13+14+15	16+17	18+19
10	12.0	200	3.4	134	8.8	38.0	21.0	5.0	6.2	42.0	6.4	35.0
20	13.4	84.0	2.3	60.5	6.4	28.6	16.8	5.9	6.7	42.0	8.4	26.9
30	11.2	40.0	1.4	31.2	1.3	16.8	8.0	12.0	6.0	30.0	13.2	24.8
40	5.3	25.0	1.0	19.3	0.38	8.8	4.0	9.0	4.8	18.8	9.5	17.5
50	2.9	17.5	0.72	13.5	2.5	7.0	2.8	3.7	3.3	14.5	4.0	10.2
60	2.2	14.0	0.76	11.2	4.2	7.1	2.4	1.1	2.9	16.8	2.9	8.4
70	2.8	12.0	0.79	9.8	4.1	7.4	2.4	0.91	6.0	20.4	2.8	8.6
80	2.9	9.0	0.68	7.5	2.0	5.6	2.5	0.88	7.4	21.6	3.3	7.4
90	2.4	6.0	0.52	5.0	0.63	3.2	2.3	1.6	6.6	18.6	4.2	5.6
100	2.4	5.1	0.51	4.3	2.0	1.8	2.4	1.6	5.6	18.4	5.1	5.1
110	2.6	5.0	0.58	4.3	3.1	2.6	2.2	0.78	3.8	15.5	4.0	4.5
120	3.2	5.6	0.76	5.1	3.2	5.5	2.4	0.64	4.4	17.6	3.6	3.9
130	4.3	6.8	1.1	6.7	2.3	9.9	3.9	2.7	8.5	26.9	5.7	7.1
135	5.9	9.0	1.7	8.9	2.2	13.5	5.4	5.5	13.0	38.7	8.6	10.8

TABLE IV. Differential cross sections at 30-eV impact energy. See Table I for the designations.

θ (deg)	DCS (10^{-19} cm^2/sr)											
	1	2	3	4	5	6	7+8	9	10+11	12+13+14+15	16+17	18+19
10	3.5	442	6.6	314	4.0	53.0	32.7	26.5	6.2	48.6	22.1	150
20	4.9	74.4	1.3	58.8	0.74	19.3	8.2	3.1	5.2	28.3	8.9	33.5
30	4.1	29.5	0.68	25.4	0.38	6.8	3.0	3.3	3.8	13.9	5.6	16.5
40	3.1	20.3	0.53	17.5	0.43	3.9	2.2	3.7	3.7	11.6	4.7	14.2
50	1.9	13.3	0.37	11.7	0.69	3.2	1.9	2.7	3.5	11.2	3.9	10.9
60	0.96	7.7	0.23	6.9	1.1	3.1	1.5	1.4	3.5	11.6	3.1	7.5
70	0.43	3.6	0.12	3.3	0.90	2.3	1.0	0.11	3.0	10.4	1.9	4.3
80	0.43	2.4	0.09	2.2	0.55	1.8	0.84	0.23	3.1	9.4	1.6	3.1
90	0.50	2.1	0.10	1.9	0.19	1.3	0.71	1.1	2.5	6.5	1.7	2.7
100	0.54	1.8	0.10	1.6	0.17	1.0	0.50	1.5	1.4	4.3	1.7	2.2
110	0.99	2.6	0.19	2.3	0.33	1.5	0.65	2.5	1.4	4.9	2.5	2.9
120	1.10	2.5	0.24	2.2	0.35	1.8	0.73	2.5	1.3	5.0	2.5	2.4
130	1.00	2.0	0.24	1.8		2.1	0.74	1.8	1.5	5.0	1.9	1.6
135	(1.0)	(1.8)	(0.25)	(1.6)		(2.3)	(0.76)	(1.5)	(1.4)	(5.4)	(1.7)	(1.4)

TABLE V. Differential cross sections at 50-eV impact energy. See Table I for the designations.

θ (deg)												
	1	2	3	4	5	6	7+8	9	10+11	12+13+14+15	16+17	18+19
10	8.2	510	3.3	418	3.1	56.1	33.2	28.1	10.2	56.1	25.5	337
20	3.0	100	0.90	88.0	1.0	26.0	11.0	5.5	4.5	30.0	13.0	97.0
30	1.2	25	0.33	21.5	0.38	3.5	1.8	5.0	2.4	9.0	6.3	28.0
40	0.40	8.3	0.15	7.7	0.19	1.2	0.81	2.7	1.3	3.4	2.4	9.0
50	0.24	3.6	0.08	3.2	0.11	0.94	0.65	1.2	1.2	4.0	1.6	4.7
60	0.25	1.9	0.050	1.7	0.080	0.87	0.44	0.53	1.2	4.4	1.3	3.0
70	0.14	1.1	0.030	0.98	0.053	0.57	0.18	0.66	0.52	2.0	0.85	1.7
80	0.17	1.5	0.044	1.3	0.075	0.72	0.23	1.4	0.39	1.6	1.0	1.8
90	0.18	1.5	0.050	1.3	0.11	0.63	0.26	1.7	0.32	1.2	1.1	1.4
100	0.16	1.0	0.040	0.89	0.094	0.36	0.17	1.2	0.23	0.76	0.90	0.86
110	0.18	0.70	0.036	0.64	0.084	0.24	0.11	0.91	0.21	0.53	0.63	0.60
120	0.19	0.46	0.032	0.42	0.074	0.16	0.055	0.64	0.20	0.48	0.60	0.42
130	0.21	0.30	0.026	0.27	0.078	0.10	0.029	0.38	0.20	0.51	0.39	0.33
135	0.20	0.24	0.024	0.22	0.082	0.082	0.021	0.26	0.20	0.55	0.30	0.30

TABLE VI. Differential cross sections at 100-eV impact energy. See Table I for the designations.

	DCS (10^{-19} cm^2/sr)							
θ (deg)	2	4	6	9	10+11	12+13+14+15	16+17	18+19
10	150	126	18.0	9.0	3.0	15.0	9.8	128
20	15.0	13.2	3.6	2.9	0.75	3.5	5.3	12.8
30	5.6	5.0	1.3	2.6	0.56	2.4	3.1	6.8
40	1.4	1.2	0.28	1.0	0.27	0.84	0.91	2.0
50	0.68	0.62	0.12	0.64			0.48	1.1
60	0.50	0.48	0.08	0.58				
70	0.46	0.40	0.06	0.64				
80	0.50	0.37	0.05					
90	0.68		0.03					

(features 12, 13, 14, 15). It was necessary, however, to retain the 19 individual features in the computer treatment of the data because the width of the combined features was much larger than the width of a well-separated individual feature.

The relative inelastic-scattering intensities with respect to the $5s[1\frac{1}{2}]_1$ excitation (feature 2) have been obtained from each spectrum and the 20-eV ratios are shown as a function of scattering angle in Figs. 6 through 9. Smooth curves have been drawn through the experimental points and these curves have been accepted as the ratios for the purpose of obtaining the DCS. The scatter of the data points and the shapes of DCS curves are typical for the many other ratios which are not presented here.

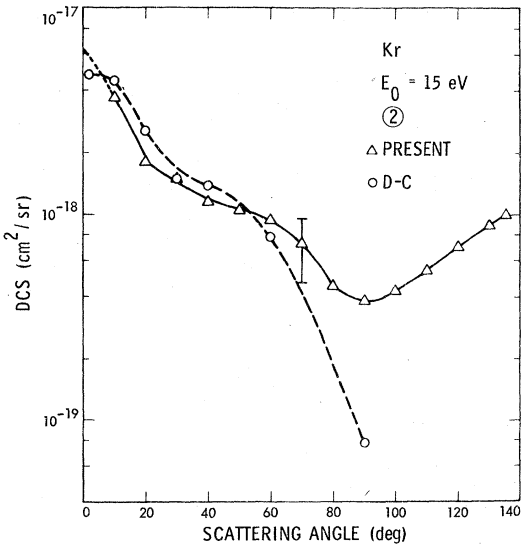

FIG. 4. Differential cross sections for the excitation of the $5s[1\frac{1}{2}]_1$ state at 15-eV impact energy. Present results, △; Delage and Carette (Ref. 16), ○. A smooth curve was drawn through the present DCS points. The relative values of Delage and Carette (Ref. 16) have been normalized to the present data at 30°.

Relative scattering intensities meaured by Delage and Carette,[16] normalized to the present results at specific angles, are also shown for the purpose of comparison in Figs. 6–9. There is reasonably good agreement between the two measurements although occasional deviations by about a factor of 2 occurs, mainly for the weaker transitions.

C. Differential cross sections

Absolute DCS values were obtained from the ratios by utilizing the absolute values of the $5s[1\frac{1}{2}]_1$ transition. The resulting absolute inelastic DCS

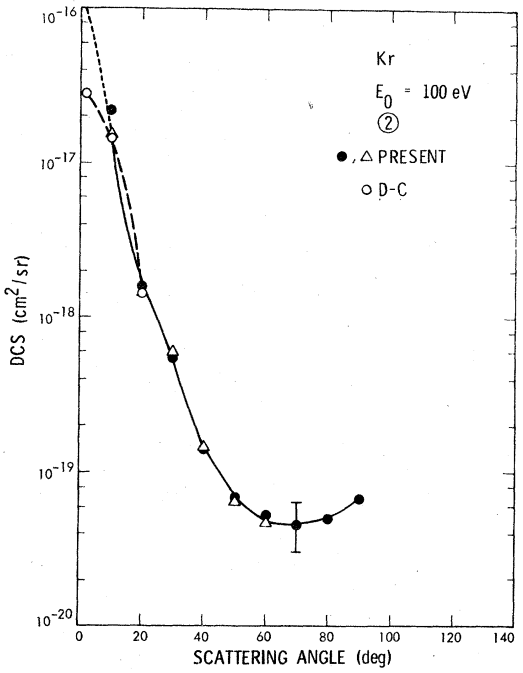

FIG. 5. Same as Fig. 3 except E_0=100 eV. The relative values of Delage and Carette (Ref. 16) in this case were normalized to the present data at 20°. Two sets of measurements are shown to indicate the reproducibility of the present data.

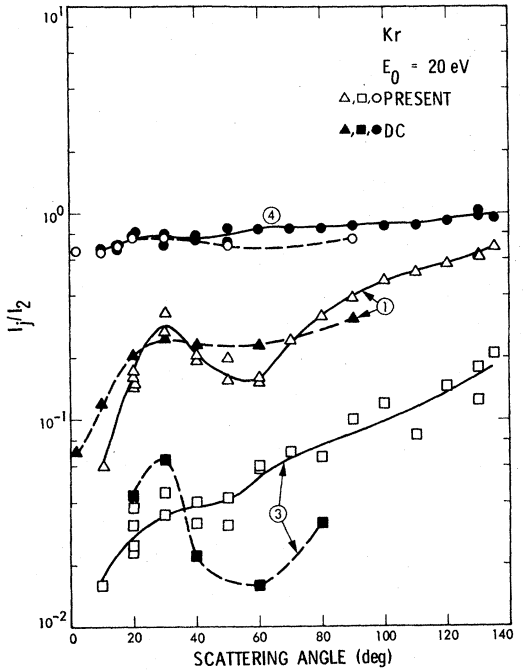

FIG. 6. Relative inelastic-scattering intensities at 20-eV impact energy. j refers to the number of the features (see Table I). In the figures these numbers appear in the circles. The results of Delage and Carette (Ref. 13) (DC) are compared with the present data.

are summarized in Tables II to VI and the 20-eV results are shown in Figs. 10 to 13. The inelastic DCS's for angles less than 10° represent extrapolated values and no measurements were carried out for angles greater than 135°. At 100-eV impact energy the intensity at high scattering angles was quite weak and consequently measurements could not be made for angles greater than 90°.

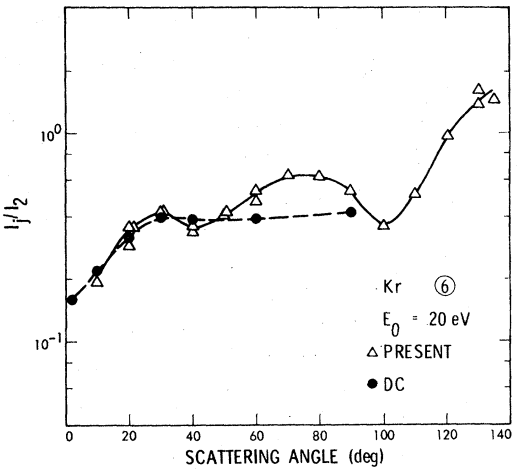

FIG. 8. Same as Fig. 6 except for the feature 6.

There is a good agreement in the angular behavior of the $4p \rightarrow 5s$ unresolved excitation at 50-eV impact energy between the results of Lewis *et al.*[11] and the present results (features 1, 2, 3, and 4 added together). However, Lewis *et al.* carried out an approximate normalization of their relative measurements to results obtained using an optical-model theory which yielded cross sections by about a factor 4 lower than the present results. With the exception of the $5s[1\frac{1}{2}]_1$ state, no other data (either experimental or theoretical) are available to which the present data can be compared. The optically allowed $5s[1\frac{1}{2}]_1$ and $5s'[0\frac{1}{2}]_1$ excitation DCS's are usually the largest at all energies and show considerable forward peaking character especially at higher impact energies. The $5p[0\frac{1}{2}]_0$

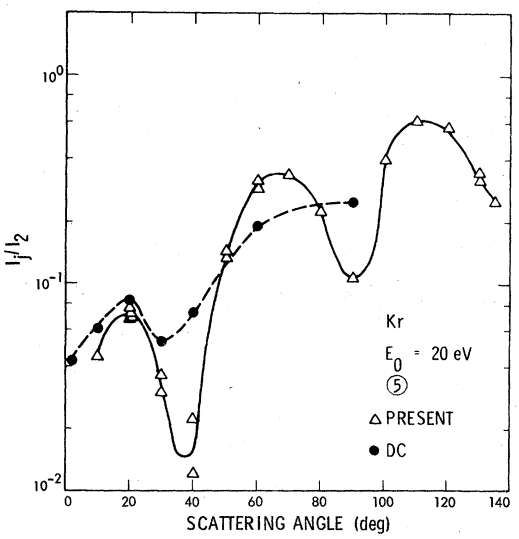

FIG. 7. Same as Fig. 6 except for the feature 5.

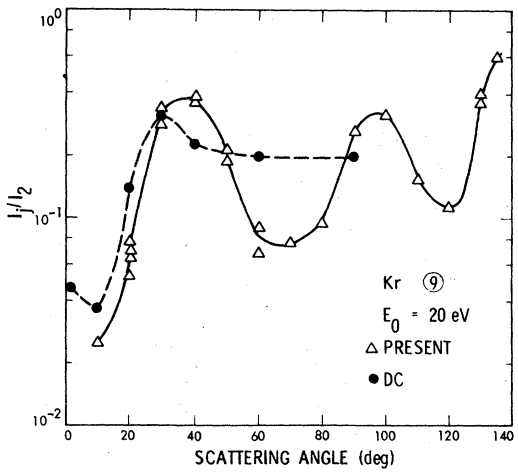

FIG. 9. Same as Fig. 6 except for the feature 9.

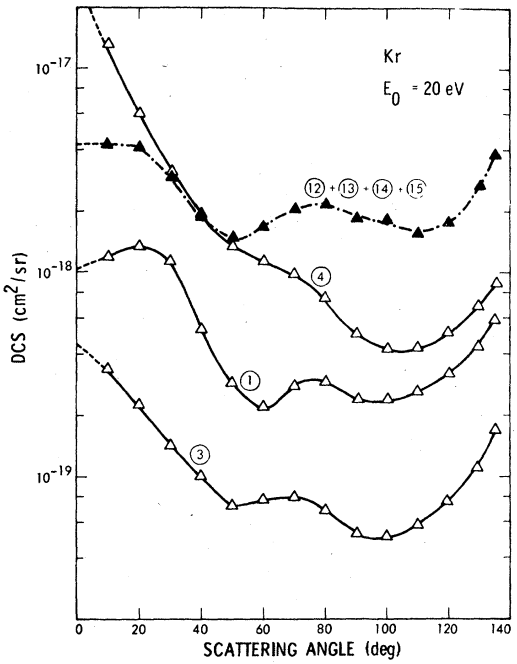

FIG. 10. Differential cross sections for excitation of various electronic states at 20-eV impact energy. See Table I for designations. The experimental data points have been connected by smooth curves.

excitation cross section shows a deep minimum at high scattering angles which shifts to lower angles with increasing impact energy and at the same time becomes less pronounced. The other DCS's are more difficult to characterize in simple

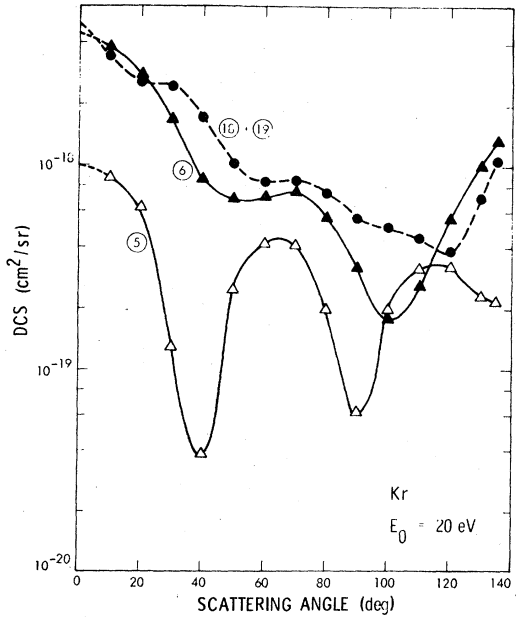

FIG. 11. Same as Fig. 10.

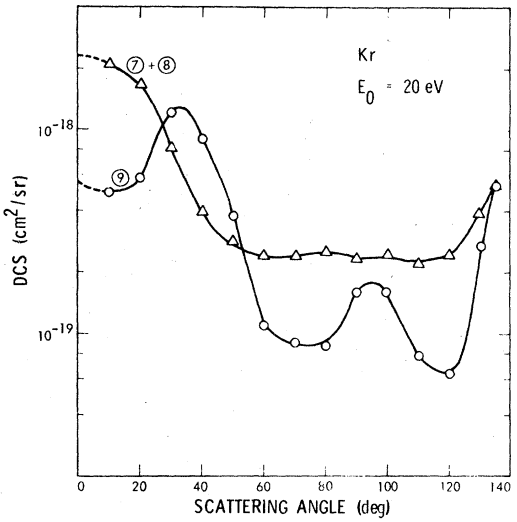

FIG. 12. Same as Fig. 10.

terms because they change significantly with angle and energy and many of them represent the combination of more than one excitation process.

The energy dependence of DCS for $5s[1\frac{1}{2}]_2$, and $5s[1\frac{1}{2}]_1$ excitations at several scattering angles are shown in Figs. 14 and 15. The cross section for the optically forbidden $5s[1\frac{1}{2}]_2$ transition is small at every energy and peaks at low energies especially at higher scattering angles. The optically allowed $5s[1\frac{1}{2}]_1$ DCS peak at somewhat higher energy, as expected, but this maximum shifts closer to threshold with increasing scattering angles. The drawing of the curves through the 20° and 30° DCS are somewhat arbitrary. The minima at around 40-eV impact energy have not been carefully investigated. The error limits are comparable to the oscillation but there seem to be a definite indication for at least some local minimum.

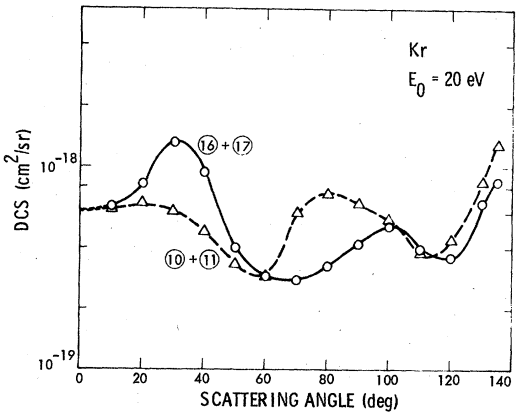

FIG. 13. Same as Fig. 10.

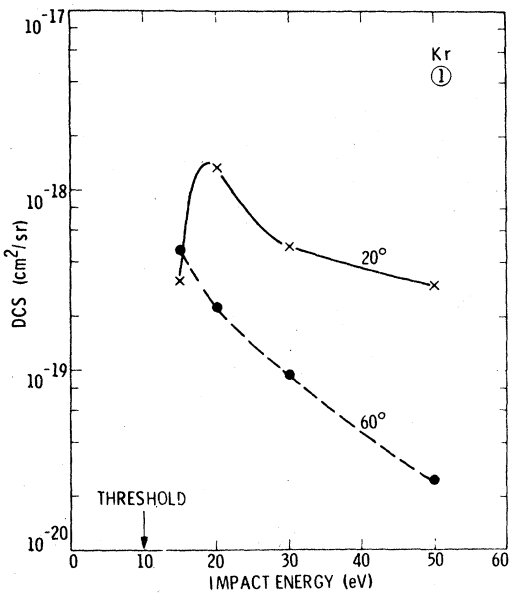

FIG. 14. Energy dependence of the differential cross section for the $5s[1\frac{1}{2}]_2$ excitation process at 20° and 60° scattering angles. Smooth curves were drawn through the experimental points.

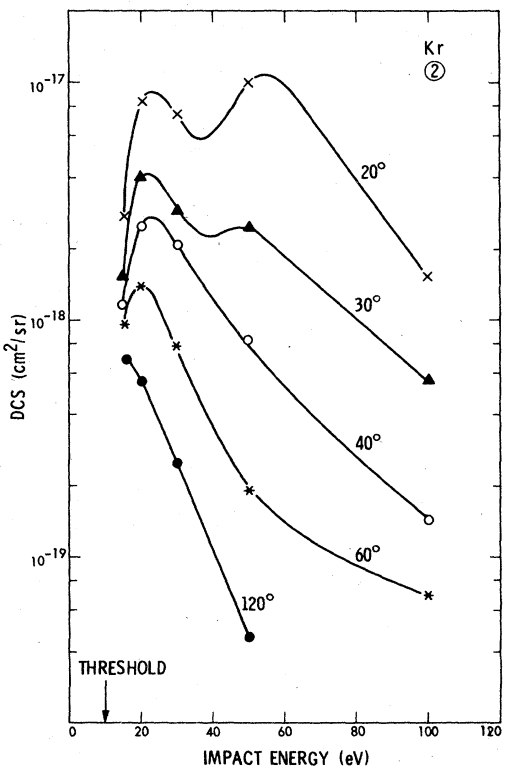

FIG. 15. Energy dependence of the differential cross section for the $5s[1\frac{1}{2}]_1$ excitation process at 20°, 30°, 40°, 60°, and 120° scattering angles. Smooth curves were drawn through the experimental points.

D. Integral elastic and momentum transfer cross sections

The DCS's for the various excitation processes have been extrapolated to 0° and to 180° scattering angles and integrated to obtain integral and momentum-transfer cross sections. The extrapolation to 0° was aided by theoretical predictions and experience with other rare gases. In extrapolating to 180°, we continued the tendency of the curves from 135° to 140° smoothly and from there to 180° the DCS was taken to be constant. This was done for the following reasons: (a) The DCS values in general are small at high angles and do not contribute much to the integral cross sections, (b) the contribution from the constant DCS section can be easily replaced by more precise values when they become available, and (c) although the momentum-transfer cross sections are more sensitive to the high-angle DCS than the integral cross sections, we simply do not know how to do the extrapolation accurately and a constant curve

TABLE VII. Summary of integral and momentum-transfer cross sections.

E_0 (eV)	Q (10^{-19} cm^2)											
	1	2	3	4	5	6	7,8	9	10,11	12,13,14,15	16,17	18,19
15	50	115	9.1	77	15	45	21	17	19	71	19	27
20	54	222	13	173	33	109	51	40	84	296	70	124
30	16	231	5.6	181	7.2	49	25	29	31	115	39	119
50	6.3	219	2.0	184	2.5	31	16	27	11	48	25	172
100		70		59		8.9		13				
	Q^M (10^{-19} cm^2)											
15	51	96	9.8	72	15	40	24	18	24	78	21	30
20	49	123	13	109	31	99	45	35	96	313	70	100
30	12	63	2.9	53	5.5	31	14	22	25	88	29	55
50	3.0	40	0.7	34	1.3	8.1	3.8	12	5.1	18	11	36
100		36		29		4.3		10				

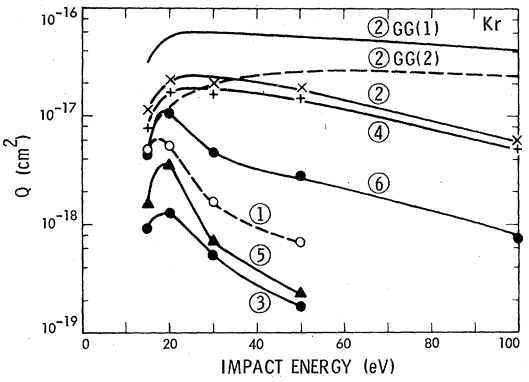

FIG. 16. Inelastic integral cross sections as a function of impact energy. See Table I for the designations. The solid and dashed curves marked as 2GG represent the calculations of GG (Ganas and Green) obtained using Born approximation and applying distortion correction, respectively. Smooth curves were drawn through the experimental points.

is as good a guess as any other. The results are summarized in Table VII and for several transitions integral cross sections are shown in Fig. 16. The optically allowed $5s[1\frac{1}{2}]_1$ and $5s'[0\frac{1}{2}]_1$ transitions dominate among the inelastic processes at all energies and especially at higher impact energies. Many of the excitation cross sections peak just a few eV above threshold resembling optically forbidden spin exchange transitions. The theoretical values for the $5s[1\frac{1}{2}]_1$ excitation obtained by Ganas and Green[15] are also shown for comparison. The upper curve has been obtained with the Born scattering approximation while for the lower curve a distortion correction was made. No other theoretical or experimental data are available to which the present results could be compared. The inelastic momentum-transfer cross sections are about an order of magnitude smaller for the $5s[1\frac{1}{2}]_1$ and $5s'[0\frac{1}{2}]_1$ excitation than for that due to elastic scattering. The other inelastic processes have even smaller momentum-transfer cross sections.

E. Error estimation

The errors associated with the present DCS have been estimated on the basis of the elastic DCS errors and on the scatter in the intensity ratio measurements. The relative value of the inelastic DCS are estimated to be accurate to within ±15%, the inelastic to elastic intensity ratios to within ±25%, and the elastic DCS have been claimed to be accurate within ±20%. The overall errors calculated as the square root of the sum of the squares of the individual errors is, therefore ±35% for the present DCS. Additional uncertainties contribute to the integral and momentum-transfer cross sections due to extrapolations. We estimate these errors to be about 15% and 30%, respectively. Combining this with the DCS uncertainties the error limits on the integral and momentum transfer cross sections are 38% and 46%, respectively.

ACKNOWLEDGMENTS

We would like to express our gratitude to J. D. Carette and E. Weigold for sending us their cross-section values. This research was supported in part by the National Aeronautics and Space Administration, Contract No. NAS7-100 and in part by the Department of Energy, Order No. LS-76-5. Two of us (H.T. and H.N.) are grateful to NRC and NASA for financial support.

*Permanent address: Department of Physics, Sophia University, Tokyo, Japan.
†Permanent address: Department of Physics, Faculty of Science, Niigata University, Ikarashi, Niigata 950-21, Japan.

[1]M. L. Bhaumik, R. S. Bradford, Jr., and E. R. Ault, Appl. Phys. Lett. 28, 23 (1976).
[2]R. S. Bradford, Jr., W. B. Lacina, W. H. Long, Jr., J. B. West, and M. L. Bhaumik, NRTC Report No. 77-15R (unpublished).
[3]S. K. Srivastava, H. Tanaka, A. Chutjian, and S. Trajmar, Phys. Rev. A 23, 2167 (1981).
[4]A. Chutjian and D. C. Cartwright, Phys. Rev. A 23, 2178 (1981).
[5]C. Ramsauer, Ann. Phys. (Leipzig) 72, 345 (1923).
[6]C. Ramsauer and R. Kollath, Ann. Phys. Leipzig 3, 536 (1929).
[7]H. S. W. Massey, E. H. S. Burhap, and H. B. Gilbody, *Electronic and Ionic Impact Phenomena*, (Oxford University Press, Oxford, 1969), Vol. I, p. 25.
[8]M. Schaper and H. Scheibner, Beitr. Plasmaphys. 9, 45 (1969).
[9]R. W. Wagenaar, FOM Report No. 34.948 and R. W. Wagenaar and F. J. de Heer, J. Phys. B 13, 3855 (1980).
[10]F. J. de Heer, R. H. J. Jansen, and W. van der Kaay, J. Phys. B 12, 979 (1979).
[11]B. R. Lewis, E. Weigold, and P. J. O. Teubner, J. Phys. B 8, 212 (1975); E. Weigold (private communication).
[12]B. R. Lewis, I. E. McCarthy, P. J. O. Teubner, and E. Weigold, J. Phys. B 7, 2549 (1974).
[13]A. Delage and J. D. Carette, Can. J. Phys. 53, 2079 (1975).
[14]A. Delage and J. D. Carette, J. Phys. B 9, 2399 (1976).
[15]P. S. Ganas and A. E. S. Green, Phys. Rev. A 4, 182

(1971).
[16]A. Delage and J. D. Carette, Can. J. Phys. 55, 1835 (1977); J. D. Carette (private communication).
[17]J. Geiger, Phys. Lett. 33A, 351 (1970).
[18]J. P. De Jongh and J. Van Eck, Physica (Utrecht) 51, 104 (1971).
[19]A. Chutjian, J. Chem. Phys. 61, 4279 (1974).
[20]D. C. Cartwright, A. Chutjian, S. Trajmar, and W. Williams, Phys. Rev. A 16, (1977).
[21]S. Trajmar, D. C. Cartwright, and W. Williams, Phys. Rev. A 4, 1482 (1971).